JACS
JOURNAL OF THE AMERICAN CHEMICAL SOCIETY

Article

Tetrahedral Geometry Induction of Stable Ag-Ti Nanoclusters by Flexible Trifurcate TiL3 Metalloligand

Mei-Yan Gao, Kai Wang, Yayong Sun, Dejing Li, Bai-Qiao Song, Yassin H. Andaloussi, Michael J. Zaworotko, Jian Zhang, and Lei Zhang

J. Am. Chem. Soc., **Just Accepted Manuscript** • DOI: 10.1021/jacs.0c05199 • Publication Date (Web): 24 Jun 2020

Just Accepted

is published by the American Chemical Society. 1155 Sixteenth Street N.W., Washington, DC 20036

Tetrahedral Geometry Induction of Stable Ag-Ti Nanoclusters by Flexible Trifurcate TiL_3 Metalloligand

Mei-Yan Gao,[a, b] Kai Wang,[a] Yayong Sun,[a] Dejing Li,[a] Bai-Qiao Song,[b] Yassin H. Andaloussi,[b] Michael J. Zaworotko,[b] Jian Zhang[a] and Lei Zhang*[a]

[a] State Key Laboratory of Structural Chemistry, Fujian Institute of Research on the Structure of Matter, Chinese Academy of Sciences, Fuzhou, Fujian, P. R. China 350002.

[b] Department of Chemical Sciences, Bernal Institute, University of Limerick, Limerick, Republic of Ireland.

ABSTRACT: A series of increasingly large silver nanoclusters with a varied combination of Archimedean and/or Platonic solid arrangements were constructed using a flexible trifurcate TiL_3 (L = Salicylic acid or 5-fluorosalicylic acid) metalloligand: $Ag_4@Ag_4@Ti_4$ (**PTC-85**), $Ag_{12}@Ti_4$ (**PTC-86**), $Ag_4@Ag_6@Ag_{12}@Ti_4$ (**PTC-87**), $Ag_6@Ag_{24}@Ag_{12}@Ti_4$ (**PTC-88**) and $Ag_{12}@Ag_{24}@Ti_4$ (**PTC-89**). The silver nanoclusters are each capped by four TiL_3 moieties, thereby forming $\{Ti_4\}$ supertetrahedra with average edge lengths ranging from ~ 8.12 Å to ~ 17.37 Å. Such $\{Ti_4\}$ moieties further induce the tetrahedral geometry of the encapsulated silver nanoclusters. These atomically precise metallic clusters were found to be ultra-stable with respect to air for several months, and to water for more than 3 days, due to the stabilizing effects of the TiL_3 metalloligand. Moreover, the obtained clusters exhibit non-linear optical (NLO) effects in optical limiting tests and also temperature-dependent photoluminescent properties. This work provides an interesting metalloligand method not only to induce the spatial growth of metallic clusters to achieve highly symmetric structures, but also to enhance their stability which is crucial for future application.

INTRODUCTION

Supramolecular assemblies have garnered increasing attention in recent years due to the elegant structures and distinctive properties that may be designed.[1-7] In the field of metal-based nanoclusters, the use of self-assembly from building blocks with directional features has resulted in assemblies that exhibit polyhedral geometry, including Archimedean and Platonic solids.[8-16] Metalloligands are powerful tools for this purpose whereby the predictable coordination geometries of metal complexes can be exploited for the construction of successively complicated supramolecules.[17-22] During our recent studies on titanium-organic coordination cages, titanium ions were found to reliably bind to 2-hydroxybenzoic acids to form stable chelate complexes.[23, 24] As such, titanium-based metalloligands with trifurcate TiL_3 moieties (L= salicylate or 5-fluorosalicylate), could be envisaged to be well-suited for the controlled formation and stabilization of metallic nanoclusters (Scheme 1) owing to their conformational flexibility.

Silver nanoclusters are of particular interest because of their potential catalytic and photoactive properties. While a large number of Ag nanoclusters have previously been reported, with some displaying particularly high symmetry, the controlled growth of high nuclearity and high symmetry families of clusters still remains a challenge.[25-29] The use of structure-directing additives such as the highly directional nature of metalloligands can play a significant role in the design of high-performance nanoclusters.[17, 19] However, research efforts in this field have also been deeply frustrated by the generally poor stability of polysilver nanoclusters, which in turn hinders full characterization and utility.[30-33] As mentioned above, TiL_3 metalloligands based upon salicylate and 5-fluorosalicylate can generate titanium metalloligands which possess three uncoordinated carbonyl groups to form trifurcated bridging to cap metallic nanoclusters. Herein, we address the rational growth matter of silver clusters through the use of TiL_3 metalloligands to induce their symmetric growth and enhance their stability.

Scheme 1. Illustration of tetrahedral geometry induction of Ag nanoclusters by the trifurcate TiL_3 metalloligands.

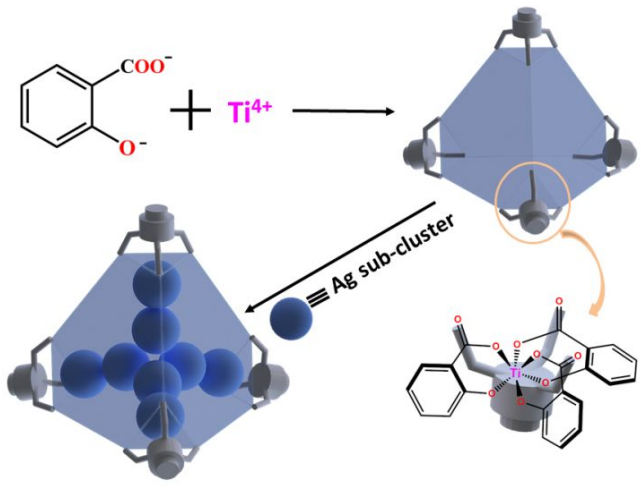

In this work, a family of five novel heterometallic Ag-Ti clusters with tetrahedral geometry were assembled *via* the flexible trifurcate TiL_3 metalloligand: $Ti_4Ag_8(SA)_{12}$•MeOH (H_2SA = salicylic acid, **PTC-85**), $Ti_4Ag_{12}(S^iPr)_6(SA)_{10}(HSA)_2$•$H_2O$ (**PTC-86**), $Ti_4Ag_{22}(S^iPr)_{12}(SA)_{12}SO_4$ (**PTC-87**), $Ti_4Ag_{42}(S)_4(S^iPr)_{18}(SA)_{12}(SO_4)_4$•8MeOH (**PTC-88**) and $Ti_4Ag_{36}(S^iPr)_{24}$(SA-F)$_{12}(SO_4)_2$ (H_2SA-F = 5-fluorosalicylic acid, **PTC-89**), abbreviated as $Ag_4@Ag_4@Ti_4$, $Ag_{12}@Ti_4$, $Ag_4@Ag_6@Ag_{12}@Ti_4$, $Ag_6@Ag_{24}@Ag_{12}@Ti_4$ and $Ag_{12}@Ag_{24}@Ti_4$, respectively. The average lengths of each {Ti_4} tetrahedra edge ranges from 8.12 Å to 17.37 Å. In addition, the core of the five clusters is comprised of tetrahedral arrangements of polysilver cores based upon Platonic (tetrahedron, octahedron) polyhedra and/or Archimedean (truncated tetrahedron, cuboctahedron, truncated octahedron) solids. These nanoclusters demonstrate ultra-stability in air for several months and in water over 3 days due to the encapsulation effects of the trifurcate TiL_3 metalloligands. Moreover, **PTC-85**, **PTC-86** and **PTC-89** exhibited variable photoluminescent properties at different temperatures. **PTC-85**, **PTC-87** and **PTC-89** were also found to display optical limiting properties.

EXPERIMENTAL SECTION

The precursors of [Ag(^{i}PrS)]n were prepared according to the literature.[26] All reagents and solvents employed were purchased commercially and used as received without further purification. Ti(O^iPr)$_4$, glacial acetic acid and 5-fluorosalicylic acid were purchased from Aladdin, salicylic acid, CH_2Cl_2 and ^{i}PrOH were acquired from from Adamas-beta, while AgOAc, DMF, CH_3OH, $AgNO_3$, Ag_2SO_4, $AgClO_4$, N_2H_4 and formic acid were bought from Sinopharm Chemical Reagent Beijing. Fourier transform infrared spectroscopy (FT-IR) data were collected on a PerkinElmer Spectrum 100 FT-IR Spectrometer. The UV diffuse reflection data were recorded at room temperature using a powder sample with $BaSO_4$ as a standard (100% reflectance) on a PerkinElmer Lamda-950 UV spectrophotometer. Powder X-ray diffraction (PXRD) analysis was performed on a MiniFlex2 X-ray diffractometer using Cu-Kα radiation (λ = 0.1542 nm) in the 2θ range of 5–50° with a scanning rate of 5° min−1. The thermogravimetric analyses (TGA) were performed on a Mettler Toledo TGA/SDTA 851e analyzer in N_2 atmosphere with a heating rate of 10 °C/min from 20°C to 800°C. Elemental analyses (C, H, and S) were carried out on a Vario Micro E III analyzer. X-ray photoelectron spectroscopy (XPS) analysis was carried out on Thermo Scientific Escalab 250Xi spectrometer. Electrospray ionization mass spectrometry (ESI-MS) measurements were performed on a mass spectrometer (JEOL AccuTOF 4G LC-plus). Fluorescence spectra were measured with a HORIBA Jobin-Yvon FluoroMax-4 spectrometer from 77 to 298 K in the solid state. The experimental Ti:Ag ratios were measured by inductively coupled plasma (ICP) atomic emission spectroscopy analysis (Table S3).

Synthesis of Ti(SA)$_3$ metalloligand: Salicylic acid (1.50 g, 0.011 mol) and AgOAc (0.10 g, 0.22 mmol) were added to 8.0 mL of DMF:CH_3CN (v:v = 3:5); then Ti(O^iPr)$_4$ (0.50 mL, 1.50 mmol) was added. The solution was then sealed in a 20 mL vial and transferred to a preheated oven heated to 80 °C for around 3 days. After cooling to room temperature, the solution was slowly evaporated at room temperature to yield red block crystals of **Ti(SA)$_3$** in high purity with a yield of ~80% based on Ag.

Synthesis of PTC-85: AgOAc (0.10 g, 0.60 mmol), salicylic acid (1.50 g, 0.011 mol) and 0.12 mL of formic acid were added to 8.0 mL of DMF:CH_3OH (v:v = 3:5); then Ti(O^iPr)$_4$ (0.50 mL, 1.50 mmol) was added. The resultant solution was filtered through a 0.45 μm syringe filter. The solution was then sealed in a 20 mL vial and transferred to a preheated oven heated to 80 °C for around 12 hours. After cooling to room temperature, the solution was slowly evaporated at room temperature to yield red needle crystals of **PTC-85** in high purity with a yield of ~50% based on Ag. Elemental analysis (%) for $C_{85}H_{56}Ag_8O_{41}Ti_4$, calc: C, 36.62; H, 20.25. Found: C, 36.12; H, 21.08.

Synthesis of PTC-86: [Ag(^{i}PrS)]n (0.024 g, 0.013 mmol), $AgClO_4$ (0.052 g, 0.25 mmol), salicylic acid (1.50 g, 0.011 mol), 0.50 mL of H_2O and 1 drop N_2H_4 were added to 8.0 mL of glacial acetic acid; then Ti(O^iPr)$_4$ (0.04 mL, 0.14 mmol) was added. The resultant solution was filtered through a 0.45 μm syringe filter. The solution was then sealed in a 20 mL vial and transferred to a preheated oven heated to 80 °C for around 12 hours. After cooling to room temperature, the solution was slowly evaporated at room temperature to yield red cubic crystals of **PTC-86** in high purity with a yield of ~65% based on Ag. Elemental analysis (%) for $Ag_{12}C_{102}O_{37}S_6Ti_4H_{94}$, calc: C, 34.12; H, 2.63; S, 5.36. Found: C, 33.84; H, 2.75; S, 5.21.

Synthesis of PTC-87: [Ag(^{i}PrS)]n (0.06 g, 0.33 mmol), Ag_2SO_4 (0.07 g, 0.22 mmol), salicylic acid (1.50 g, 0.011 mol) and 0.12 mL of formic acid were added to 10.0 mL of CH_3COOH:CH_2Cl_2 (v:v = 8:2); then Ti(O^iPr)$_4$ (0.50 mL, 1.76 mmol) was added. The resultant solution was filtered through a 0.45 μm syringe filter. The solution was then sealed in a 20 mL vial and transferred to a preheated oven heated to 80 °C for around 12 hours. After cooling to room temperature, the solution was slowly evaporated at room temperature to yield red block crystals of **PTC-87** in high purity with a yield of ~45% based on Ag. Elemental analysis (%) for $Ag_{22}C_{120}O_{40}S_{13}Ti_4H_{132}$, calc: C, 27.74; H, 2.56; S, 8.02. Found: C, 27.88; H, 2.62; S, 7.91.

Synthesis of PTC-88: [Ag(^{i}PrS)]n (0.06 g, 0.33 mmol), Ag_2SO_4 (0.07 g, 0.22 mmol), salicylic acid (1.50 g, 0.011 mol) and 0.12 mL of formic acid were added to 8.0 mL of ^{i}PrOH:CH_3OH (v:v = 3:5); then Ti(O^iPr)$_4$ (0.50 mL, 1.76 mmol) was added. The solution was then sealed in a 20 mL vial and transferred to a preheated oven heated to 80 °C for around 12 hours. After cooling to room temperature, the solution was slowly evaporated at room temperature to yield red octahedral crystals of **PTC-88** with a yield of ~5% based on Ag.

Synthesis of PTC-89: [Ag(^{i}PrS)]n (0.06 g, 0.33 mmol), Ag_2SO_4 (0.07 g, 0.22 mmol), 5-fluorosalicylic acid (1.50 g, 0.008 mol) and 0.10 mL of formic acid were added to 8.0 mL of ^{i}PrOH:CH_3OH (v:v = 3:5); then Ti(O^iPr)$_4$ (0.50 mL, 1.76 mmol) was added. The solution was then sealed in a 20 mL vial and transferred to a preheated oven heated to 80 °C for around 12 hours. After cooling to room temperature, the solution was slowly evaporated at room temperature to yield

red plate crystals of **PTC-89** in high purity with a yield of ~56% based on Ag. Elemental analysis (%) for $C_{156}O_{44}S_{26}Ti_4Ag_{36}F_{12}H_{204}$, calc: C, 23.66; H, 2.60; S, 10.53. Found: C, 23.26; H, 2.51; S, 10.47.

X-ray Crystallography. Crystallographic data for **PTC-85, PTC-86, PTC-87** and **PTC-89** were collected on a Rigaku MM007-Saturn724+ diffractometer equipped with graphite-monochromated Mo Kα radiation source (λ = 0.71073 Å) at room temperature (293K). Crystallographic data for **PTC-88** was collected on a Supernova single crystal diffractometer equipped with graphite-monochromated Cu Kα radiation source (λ = 1.54178 Å) at low temperature (100K). Absorption correction was applied using SADABS.[34] Structures were solved by direct methods and refined by full-matrix least-squares on F^2 using SHELXTL-2014 and Olex 2.[35, 36] Non-hydrogen atoms were refined anisotropically, and all hydrogen atoms were generated geometrically. The SQUEEZE option of PLATON was used to eliminate the contribution of disordered guest molecules to the reflection intensities.[37] CCDC 1948724-1948728 and 2009555 contains the supplementary crystallographic data for this paper. These data are provided free of charge by The Cambridge Crystallographic Data Centre.

Z-scan Measurements. The nonlinear optical property of the samples was evaluated using the open-aperture (OA) Z-scan technique. The excitation light source was an Nd:YAG laser with a repetition rate of 10 Hz. The laser pulses (with a period of 8.5 ns and 532nm wavelength) were split into two beams with a mirror. The pulse energies at the front and back of the samples were monitored using energy detectors D1 and D2. All of the measurements were conducted at room temperature. Crystalline samples were dissolved in DMF (3 mg/mL). The sample was mounted on a computer-controlled translation stage that shifted each sample along the z-axis.

RESULTS AND DISCUSSION

Through a solvothermal approach at 80 °C, five red crystals of **PTC-85** to **PTC-89** were successfully assembled. These Ag-Ti nanoclusters with different sizes were constructed by varying Ag sources, using the SA or the fluorinated SA-F ligands and by altering solvent-systems. Compared to simple Ag source of AgOAc, the nuclearities of the assembled polysilver nanoclusters increased remarkably with the further addition of [Ag(^{i}PrS)]n, possibly due to the synergistic effect of different Ag sources. Besides, by substituting the SA ligands with the fluorinated SA-F, the obtained polysilver cores change from dense Ag_{42} to hollow Ag_{36} cage. Single crystal X-ray diffraction analysis revealed that they all contained polynuclear silver clusters encapsulated by apical titanium complexes (Figure 1). Each Ti cation is six-coordinate with three SA or SA-F ligands, forming the trifurcate TiL_3 metalloligand (Figure 2). Moreover, these SA or SA-F ligands offer the metalloligand a degree of flexibility to allow a variety of bonding modes to the $\{Ag_3\}$ triangular subunits that form in **PTC-85** to **PTC-89**. The TiL_3 moieties thereby serve as the capping vertices of the silver nanoclusters thereby influencing the tetrahedral structure and nuclearity of the polysilver cores. Furthermore, minor modification to the distances between the bonded silver atoms in the $\{Ag_3\}$ vertex units are shown to greatly influence the nuclearity of the assembled polysilver nanocluster. Upon decreasing the average distance of vertex silver atoms from ~4.91 Å, to ~3.21 Å and ~3.08 Å to ~3.06 Å, the nuclearity of the silver nanoclusters grows from Ag_8 (**PTC-85**), Ag_{12} (**PTC-86**) and Ag_{22} (**PTC-87**) to Ag_{42} (**PTC-88**) (Figure 2). An exception to this trend is found in the hollow cluster of **PTC-89** which has the shortest average Ag-Ag vertex distance of ~3.04 Å but middling nuclearity of Ag_{36}. Such differences may be due to the use of fluorosalicylic acid for the synthesis of **PTC-89**, which could produce different hydrophobicity and coordination environment from the salicylic acid in the preparation of **PTC-85** to **PTC-88**.

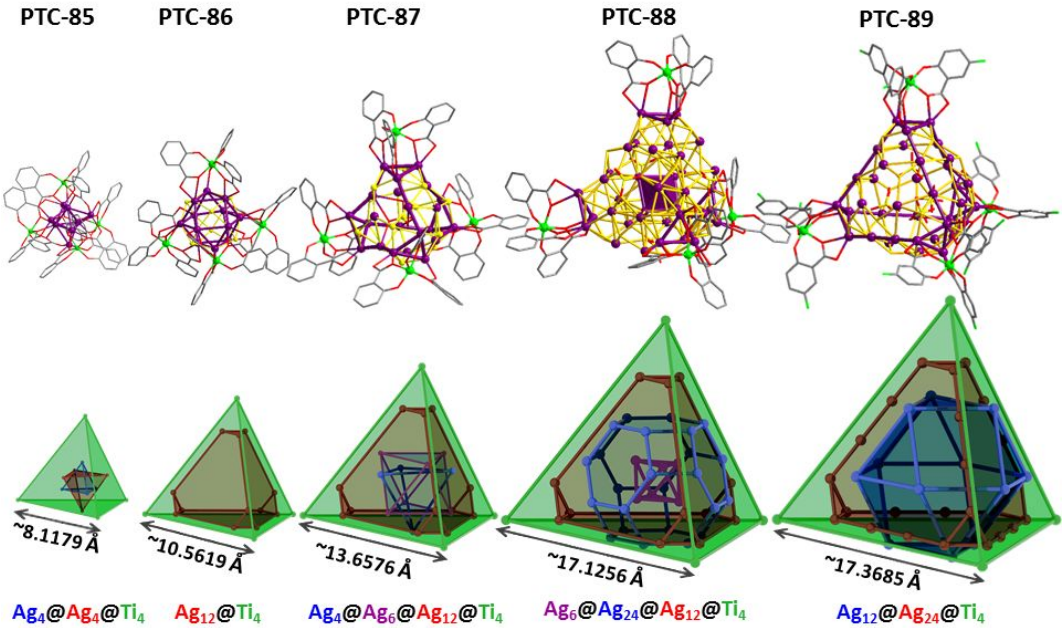

Figure 1. Molecular structures (top) and illustrations of the cluster assembly (bottom) of **PTC-85**, **PTC-86**, **PTC-87**, **PTC-88** and **PTC-89**. S^iPr^- and H atoms have been omitted for clarity. Green Ti; violet Ag; red O; yellow S; gray C.

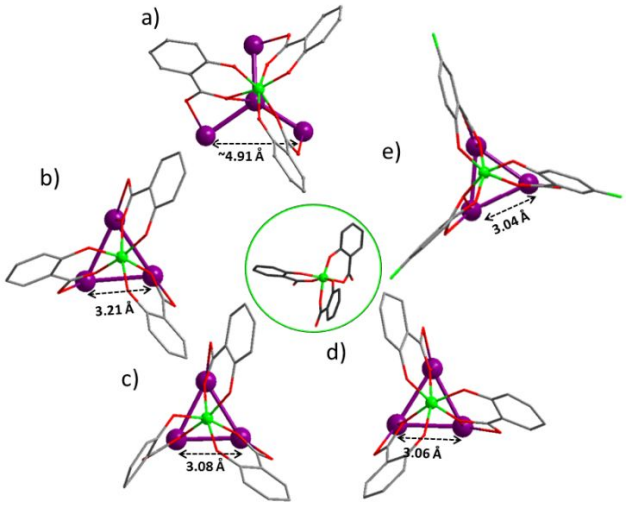

Figure 2. The structural parameters of TiL_3 metalloligands and corresponding $\{Ag_3\}$ vertex units in **PTC-85** (a), **PTC-86** (b), **PTC-87** (c), **PTC-88** (d) and **PTC-89** (e), indicating the flexibility of the TiL_3 metalloligand.

Complex **PTC-85** displays the largest Ag-Ag distance of ~4.91 Å in the $\{Ag_3\}$ vertex units (Figure 2) and the smallest cluster size (8 Ag atoms surrounded by 4 TiL_3 metalloligands) to form a tetrahedral cage with dimensions of ~8.12 Å (Ti…Ti distance). The large distance between the silver atoms coordinated to each $Ti(SA)_3$ ligand prevents direct bond formation and therefore an additional silver atom lies between each vertex creating a tetrahedron of silver atoms with average length 2.76 Å (blue tetrahedron, Figure 1 bottom left) within the 4.91 Å tetrahedron (red tetrahedron, Figure 1 bottom left). The valence states of +1 for Ag atoms were confirmed by X-ray photoelectron spectroscopy (XPS) analysis (Figure S12). Due to mutual steric hindrance between $Ti(SA)_3$ metalloligands, we speculate that 8 silver atoms is the minimum possible nuclearity for these $Ti(SA)_3$ – Ag complexes. It is noteworthy that **$Ti(SA)_3$ metalloligand** can be individually isolated. Therefore, we can also fabricate clusters of **PTC-85** by directly using the pre-synthesized **$Ti(SA)_3$ metalloligands** *via* a two-step method.

Upon decreasing the average vertex silver atom distance to ~ 3.21 Å, heterometallic nanocluster of **PTC-86** was successfully obtained forming a distorted tetrahedron made of $Ti(SA)_3$ with average lengths of ~ 10.56 Å (Ti…Ti distance) (Figures 1 and 2). The $\{Ag_{12}\}$ core in **PTC-86** forms a distorted cuboctahedron whereby each square face is capped with a deprotonated 2-propanethiol to balance the charge within the cluster (Figure S1). Unlike the reported dodecanuclear cluster $[(Ag_{12}(S^tBu)_6(CF_3COO)_6(CH_3CN)_6]\cdot CH_3CN)]$[33], **PTC-86** exhibited excellent stability in air and water (Figure S16).

When the average distance between vertex Ag sites falls to ~ 3.08 Å, **PTC-87** forms which is composed of a tetrahedron formed from four $Ti(SA)_3$ metalloligands capping a distorted $\{Ag_{12}\}$ truncated tetrahedron whereby each triangular face is rotated with respect to a regular truncated tetrahedron (Figures 1 and 2). Within this Archimedean solid resides two Platonic solids, an $\{Ag_6\}$ octahedron and an $\{Ag_4\}$ tetrahedron. The corners of each octahedron align along the length connecting the hexagonal faces of the truncated tetrahedron, while the corners of the tetrahedron lies in the middle of the hexagonal faces. Within the core of **PTC-87** lies a tetrahedral SO_4^{2-} anion which may act as a template for this structure. The sulfate oxygen atoms point in the direction of each triangular face of the truncated tetrahedrons.[38-43] Each hexagonal face of the truncated tetrahedron hosts three 2-propanethiolate anions to give a total of twelve 2-propanethiolate anions. According to XPS analysis (Figure S13), Ag atoms in **PTC-87** also show valence states of +1, which is in agreement with those in $[SO_4@Ag_{22}(^iPrS)_{12}(NO_3)_6{\cdot}2NO_3]n$.[39]

A gigantic $(Ti(SA)_3)_4$ tetrahedra with three concentric polyhedrons form the $\{Ag_{42}\}$ core of **PTC-88** which was obtained upon the average vertex Ag-Ag distance decreasing to ~ 3.06 Å. **PTC-88** presents with $\{Ti_4\}$ tetrahedron edge lengths of ~ 17.13 Å (Ti…Ti distance) (Figures 1 and 2). **PTC-88** was obtained concurrently with **PTC-87**, but in lower yield. Single-crystal X-ray result shows that **PTC-88** crystallizes in a tetragonal unit cell (space group *I*41/*a*, a = b = 30.2914(3) Å, c = 27.4844(3) Å) (Table S2). From the outermost to the innermost polyhedrons, the three-shell $\{Ag_{42}\}$ structure of **PTC-88** consists of an $\{Ag_{12}\}$ truncated tetrahedron followed by a distorted $\{Ag_{24}\}$ truncated octahedron and finally an $\{Ag_6\}$ octahedron (Figure 1). Among these, the outermost $\{Ag_{12}\}$ truncated tetrahedron consists of 4 hexagons and 4 $\{Ag_3\}$ trigons, with each silver atom taking up a vertex. The middle $\{Ag_{24}\}$ truncated octahedron is encapsulated by the outermost $\{Ag_{12}\}$ polyhedron and is composed of 4 tetragons and 8 hexagons fused together through an edge-sharing mode with Ag atoms located at 24 vertices. In the centre of each hexagonal face, SO_4^{2-} anions act as surface ligands while also connecting the Ag polygons together by directly coordinating with two Ag atoms of the $\{Ag_{24}\}$ polygon and one Ag atom of the $\{Ag_6\}$ octahedron (Figure 3d). The $\{Ag_6\}$ octahedron is

encased within an S^{2-} tetrahedron through the capping of four of the trigonal faces (as seen in Wang et al[44]) which are then further bound to 3 Ag atoms of the truncated octahedron. Other than the four trifurcate TiL_3 metalloligands, the outer face of the $\{Ag_{42}\}$ core is decorated with 18 $^{i}PrS^{-}$ and 4 SO_4^{2-} ligands and connected together by Ag-Ag bonds and further consolidated by SO_4^{2-} ions (Figure 3).

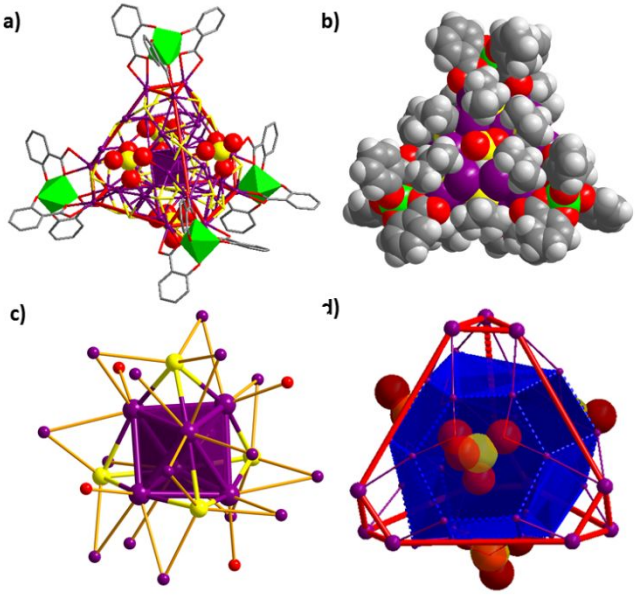

Figure 3. (a) Structure of **PTC-88** with the innermost $\{Ag_6\}$ platonic solid shown in polyhedron mode (the $S^{i}Pr^{-}$ groups are omitted); (b) Space-filling representation of **PTC-88**; (c) Coordination environment of the $\{Ag_6\}$ core in **PTC-88**; (d) Chemical bonds between the $\{Ag_{12}\}$ truncated tetrahedron and the distorted $\{Ag_{24}\}$ truncated octahedron in **PTC-88**, highlighting the four SO_4^{2-} ligands. S and O atoms are represented with the space-filling model. Green Ti; violet Ag; red O; yellow S; gray C.

Upon replacing the SA ligands with the fluorinated SA-F, a more regular tetrahedral structure in **PTC-89** was obtained in high yield with identical lengths between adjacent Ti atoms of 17.37 Å (Figures 1 and 4). As shown in Figure 1, the silver nanocluster core of **PTC-89** has 36 silver atoms and is comprised of two Archimedean solids, with each of the vertices occupied by an Ag atom. An $\{Ag_{24}\}$ truncated tetrahedron with rotationally distorted triangular faces surrounds a distorted $\{Ag_{12}\}$ cuboctahedron. Unlike the truncated tetrahedron of previous structures, 12 silver atoms form the vertices of the truncated tetrahedron while further $2 \times 6 = 12$ ones lie along the six edges of the polygon. For the $\{Ag_{12}\}$ cuboctahedron, all 12 Ag atoms account for the 12 vertices. The large void of this highly symmetric Ag-Ti nanocluster accommodates disordered SO_4^{2-} ions to balance the charge. The +1 valence states of the Ag atoms were confirmed by X-ray photoelectron spectroscopy analysis (Figure S14).The tetrahedral $\{Ag_{36}\}$ structure of **PTC-89** may also be considered to contain 4 identical bowl-like structural subunits consisting of 9 Ag atoms connected to each other by Ag-Ag bonds with same distance of 3.183 Å (Figure 4b).

From the above structural analysis, we can see that compounds **PTC-85** to **PTC-89** all share an outer tetrahedral geometry due to the induction effect of the trifurcate TiL_3 metalloligands. The application of $[Ag(^{i}PrS)]_n$ precursor and an anion template further allows the control over cluster size. Notably, the anion templating effect of SO_4^{2-} in **PTC-87** results in a higher Ag nuclearity of 22 compared to complex **PTC-86**, and the four SO_4^{2-} anions in structure **PTC-88** leads to a larger Ag nuclearity of 42. Upon changing salicylic acid to 5-fluorosalicylic acid, the symmetry and size of the polynuclear Ag core was further increased. Therefore, the trifurcate TiL_3 metalloligands induce the tetrahedral geometry of the encapsulated silver clusters, whilst the modifications to the synthetic approach influence their nuclearities.

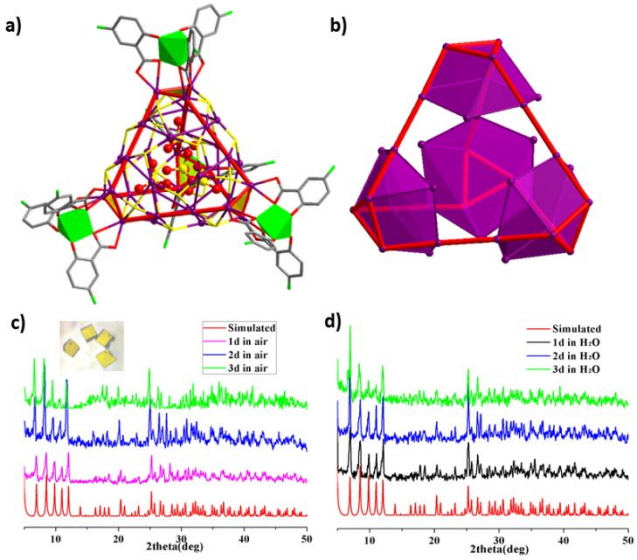

Figure 4. (a) **PTC-89** consists of an outermost tetrahedra formed from 4 Ti atoms, $\{Ag_{24}\}$ and $\{Ag_{12}\}$ Archimedean solids (the $^{i}PrS^{-}$ groups are omitted); (b) The structure of $\{Ag_{36}\}$ polyhedron in **PTC-89**; Stability tests of **PTC-89** in (c) air and (d) water.

The stability of nanoclusters is critical, as they ultimately to play a role in practical industrial applications.[45-49] Unlike many Ag-clusters which exhibit poor stability,[30-33] **PTC-85**, -**86**, -**87**, and -**89** remained stable for several months at ambient conditions and at least 3 days in water, as shown by powder X-ray diffraction (PXRD) analysis (Figures 4 and S15 to S17). Single-crystal X-ray diffraction analysis of the clusters provides a reasonable explanation for such high stability which likely arises from the fact that the outer surfaces of **PTC-85** to **PTC-89** are all surrounded by the highly-stable trifurcate TiL_3 metalloligands offering steric protection against degradation (Figure 3b and S2).

Although crystalline silver-based nanoclusters are of topical interest,[50-54] trifurcate TiL_3 metalloligand-stabilized silver nanoclusters are yet to be reported. As such, properties such as nonlinear optical (NLO) effects have not previously been studied in such clusters. Here, we conducted optical limiting measurements in DMF solutions (3 mg/mL), through open aperture (OA) Z-scan measurements. As presented in Figure 5, the Z-scan curves of **PTC-85**, **PTC-87** and **PTC-89** display reverse saturation absorption behavior. The transmittance at 532 nm of the investigated samples at the focal point reduces

to a minimum (T_{min}) from around 90% to ~ 80%. The difference between their intensities is likely from the nuclearity of the silver cores and minor differences in the trifurcate TiL_3 metalloligands, with **PTC-87** presenting the best optical limiting property. In addition, crystals of **PTC-85**, **PTC-86** and **PTC-89** show variable photoluminescent properties at different temperatures in solid state luminescence tests (Figures S18 to S20). Emission peaks of **PTC-85**, **PTC-86** and **PTC-89** were observed at ca. 500 nm (λex = 340 nm), ca. 725 nm (λex = 365 nm) and ca. 550 nm (λex = 350 nm), respectively (Figures S18 to S20). When increasing to room temperature, the emission intensity slowly decreased with the maximum emission wavelength not changing. The solution behaviors of **PTC-85** and **PTC-86** were also probed. ESI-MS spectrum of **PTC-85** in the negative mode in the solution of DMF exhibits a signal centered at m/z = 2961.86, which might be associated with the negative species of $[Ti_4Ag_8(SA)_{12}(DMF)_2(CH_3COO)]^-$ (m/z = 2960.9329) (Figures S21). Positive mode ESI-MS measurements of **PTC-86** were also carried out in the solution of DMF. It displays a signal located at m/z = 3298.0, which could be related to the $[Ti_3^{IV}Ti^{III}Ag_{12}(S^iPr)_6(SA)_{10}]^+$ fragment (m/z = 3297.85). It also shows a signal at m/z = 3222.0, which might be attributed to the segments of $[Ti_2^{IV}Ti_2^{III}Ag_{12}(S^iPr)_5(SA)_{10}]^+$ (m/z = 3222.6984) (Figures S22).

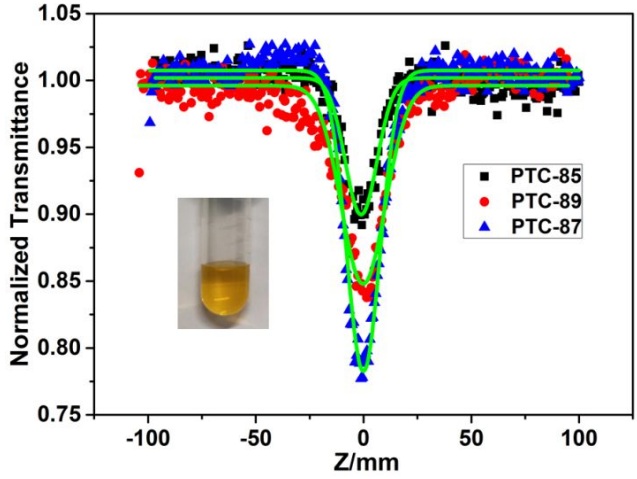

Figure 5. The open aperture Z-scan (points) and theoretical fit (solid lines) curves of **PTC-85**, **PTC-87** and **PTC-89** at 532 nm with a laser power of 120 μJ (inset: solution of **PTC-89** in DMF).

CONCLUSIONS

In summary, the flexible trifurcate TiL_3 metalloligand reported herein can serve as a structure-directing and functionalizing ligand to form a family of interesting tetrahedral nanoclusters with complicated combinations of Archimedian and Platonic solids. The structures were determined by single-crystal X-ray diffraction analysis to give core compositions of $Ag_4@Ag_4@Ti_4$, $Ag_{12}@Ti_4$, $Ag_4@Ag_6@Ag_{12}@Ti_4$, $Ag_6@Ag_{24}@Ag_{12}@Ti_4$ and $Ag_{12}@Ag_{24}@Ti_4$, which all presented tetrahedral geometry. The protective effect of the TiL_3 metalloligand makes the obtained silver nanoclusters highly stable in air and water. Furthermore, optical limiting properties and photoluminescent behaviours of these complexes were studied, which displayed noteworthy performance. The success of this work suggests that TiL_3 metalloligand might be a general structure directing agent to form highly symmetric and stable metallic nanoclusters.

ASSOCIATED CONTENT

Supporting Information. Additional figures and images; PXRD patterns, IR, solid state UV-vis absorption spectra, luminescence spectra, TGA analysis, ESI-MS spectra. This material is available free of charge via the internet at http://pubs.acs.org.

AUTHOR INFORMATION

Corresponding Author

LZhang@fjirsm.ac.cn

ACKNOWLEDGMENT

This work was supported by NSFC (21673238 and 21922111), the Strategic Priority Research Program of the Chinese Academy of Sciences (XDB20000000).

REFERENCES

[1] Liu, Y.; Hu. C.; Comotti, A.; Ward, M. D. Supramolecular Archimedean Cages Assembled with 72 Hydrogen Bonds. *Science* **2011**, *333*, 436-440.

[2] Zhang, Y.; Gan, H.; Qin, C.; Wang, X.; Su, Z.; Zaworotko, M. J. Self-Assembly of Goldberg Polyhedra from a Concave $[WV_5O_{11}(RCO_2)_5(SO_4)]^{3-}$ Building Block with 5 - Fold Symmetry. *J Am Chem Soc.* **2018**, *140*, 17365-17368.

[3] Gao, M. Y.; Wang, F.; Gu, Z. G.; Zhang, D. X.; Zhang, L.; Zhang, J. Fullerene-like Polyoxotitanium Cage with High Solution Stability. *J Am Chem Soc.* **2016**, *138*, 2556-2559.

[4] Gao, M. Y.; Fan, X.; Zhang, L.; Zhang, J. Dicarboxylate Ligands Oriented Assembly of $\{Ti_3(\mu_3\text{-}O)\}$ Units: From Dimer to Coordination Triangles and Rectangles *Inorg Chem.* **2018**, *57*, 5642-5647.

[5] Mullins, S. M.; Weissker, H. C.; Sinha-Roy, R.; Pelayo, J. J.; Garzon, I. L.; Whetten, R. L.; Lopez-Lozano, X. Chiral symmetry breaking yields the *I*-Au_{60} perfect golden shell of singular rigidity. *Nat Commun.* **2018**, *9*, 3352.

[6] Yuan, S. F.; Xu, C. Q.; Li, J.; Wang, Q. M. Ligand-Protected "Golden Fullerene": the Dipyridylamido Au_{32}^{8+} Nanocluster. *Angew.Chem. Int. Ed.* **2019**, *58*, 5906-5909.

[7] Peng, J. B.; Kong, X. J.; Zhang, Q. C.; Orendac, M.; Prokleska, J.; Ren, Y. P.; Long, L. S.; Zheng, Z.; Zheng, L. S. Beauty, Symmetry, and Magnetocaloric Effect—Four-Shell Keplerates with 104 Lanthanide Atoms. *J Am Chem Soc.* **2014**, *136*, 17938-17941.

[8] Tian, F.; Chen, R. Pd-mediated Synthesis of Ag Chiral Nanocluster with Core-shell Structure in T Point Group *J Am Chem Soc.* **2019**, *141*, 7107-7114.

[9] Byrne, K.; Zubair, Zhu, M.; N.; Zhou, X. P.; Fox, D. S.; Zhang, H.; Twamley, B.; Lennox, M. J.; Duren, T.; Schmitt, W. Ultra-large supramolecular coordination cages composed of endohedral Archimedean and Platonic bodies. *Nat Commun.* **2017**, *8*, 15268.

[10] Muller, A.; Sarkar, S.; Shah, S. Q. N.; Bogge, H.; Schmidtmann, M.; Kogerler, P.; Hauptfleisch, B.; Trautwein, A. X.; Schunemann, V. Archimedean Synthesis and Magic Numbers:

"Sizing" Giant Molybdenum-Oxide-Based Molecular Spheres of the Keplerate Type. *Angew. Chem. Int. Ed.* **1999**, *38*, 3238-3241.

[11] MacGillivray, L. R.; Atwood, J. L. A chiral spherical molecular assembly held together by 60 hydrogen bonds. *Nature* **1997**, *389*, 469-472.

[12] Rizzuto, F. J.; Wu, W. Y.; Ronson, T. K.; Nitschke, J. R. Peripheral Templation Generates an $M^{II}_6L_4$ Guest-Binding Capsule. *Angew. Chem. Int. Ed.* **2016**, *55*, 7958 –7962.

[13] Murase, T.; Nishijima, Y.; Fujita, M. Cage-Catalyzed Knoevenagel Condensation under Neutral Conditions in Water. *J Am Chem Soc.* **2012**, *134*, 162-164.

[14] Sun, Q. F.; Iwasa, J.; Ogawa, D.; Ishido, Y.; Sato, S.; Ozeki, T.; Sei, Y.; Yamaguchi, K.; Fujita, M. Self-Assembled M24L48 Polyhedra and Their Sharp Structural Switch upon Subtle Ligand Variation. *Science* **2010**, *328*, 1144-1147.

[15] Zhai, Q. G.; Bu, X.; Zhao, X.; Li, D. S.; Feng, P. Pore Space Partition in Metal–Organic Frameworks. *Acc Chem Res.* **2017**, *50*, 407-417.

[16] Pan, M.; Wu, K.; Zhang, J. H.; Su, C. Y. Chiral metal–organic cages/containers (MOCs): From structural and stereochemical design to applications. *Coord. Chem. Rev.* **2019**, *378*, 333-349.

[17] Seidel, S. R.; Stang, P. J. High-Symmetry Coordination Cages via Self-Assembly. *Acc Chem Res.* **2002**, *35*, 972-983.

[18] Olenyuk, B.; Whiteford, J. A.; Fechtenkotter, A.; Stang, P. J. Self-assembly of nanoscale cuboctahedra by coordination chemistry. *Nature* **1999**, *398*, 796-799.

[19] Leininger, S.; Fan. J.; Schmitz, M.; Stang, P. J. Archimedean solids: Transition metal mediated rational self-assembly of supramolecular-truncated tetrahedral. *PNAS.* **2000**, *97*, 1380–1384.

[20] Martir, D. R.; Cordes, D. B.; Slawin, A. M. Z.; Escudero, D.; Jacquemin, D.; Warriner, S. L.; Zysman-Colman, E. A luminescent $[Pd_4Ru_8]^{24+}$ supramolecular cage. *Chemcomn.* **2018**, *54*, 6016-6019.

[21] Li, F.; Lindoy, L. F. Metalloligand Strategies for Assembling Heteronuclear Nanocages - Recent Developments. *Aust. J. Chem.*, **2019**, *72*, 731-741.

[22] Hardy, M.; Struch, N.; Holstein, J. J.; Schnakenburg, G.; Wagner, N.; Engeser, M.; Beck, J.; Clever, G. H.; Lutzen, A. Dynamic Complex-to-Complex Transformations of Heterobimetallic Systems Influence the Cage Structure or Spin State of Iron(II) Ions. *Angew. Chem. Int. Ed.* **2020**, 59, 3195 – 3200

[23] He, Y. P.; Yuan, L. B.; Chen, G. H.; Lin, Q. P.; Wang, F.; Zhang, L.; Zhang, J. Water-Soluble and Ultrastable Ti_4L_6 Tetrahedron with Coordination Assembly Function. *J Am Chem Soc.* **2017**, *139*, 16845-16851.

[24] Zhu, B. C.; Fang, W. H.; Wang, J.; Du, Y.; Zhou, T.; Wu, K.; Zhang, L.; Zhang, J. Host-Guest and Photophysical Behavior of Ti_8L_{12} Cube with Encapsulated $[Ti(H_2O)_6]$ Species. *Chem. Eur. J.* **2018**, *24*, 14358-14362.

[25] Yonesato, K.; Ito, H.; Itakura, H.; Yokogawa, D.; Kikuchi, T.; Mizuno, N.; Yamaguchi, K.; Suzuki, K. Controlled Assembly Synthesis of Atomically Precise Ultrastable Silver Nanoclusters with Polyoxometalates. *J Am Chem Soc.* **2019**, 141, 19550-19554.

[26] Wang, Z.; Su, H. F.; Tan, Y. Z.; Schein, S.; Lin, S. C.; Liu, W.; Wang, S. A.; Wang, W. G.; Tung, C. H.; Sun, D.; Zheng, L. S. Assembly of silver Trigons into a buckyball-like Ag_{180} nanocage. *PNAS.* **2017**, *114*, 12132-12137.

[27] Li, X. Y.; Su, H. F.; Yu, K.; Tan, Y. Z.; Wang, X. P.; Zhao, Y. Q.; Sun, D.; Zheng, L. S. A platonic solid templating Archimedean solid: an unprecedented nanometre-sized Ag_{37} cluster. *Nanoscale* **2015**, *7*, 8284-8288.

[28] Cook, T. R.; Stang, P. J. Recent Developments in the Preparation and Chemistry of Metallacycles and Metallacages via Coordination. *Chem Rev.* **2015**, *115*, 7001-7045.

[29] Sun, Y.; Chen, C.; Liu, J.; Stang, P. J. Recent developments in the construction and applications of platinum-based metallacycles and metallacages *via* coordination. *Chem Soc Rev.* **2020** (DOI: org/10.1039/D0CS00038H).

[30] Abbas, M. A.; Yoon, S. J.; Khan, R.; Lee, J.; Bang, J. H. Coalescence-Driven Simultaneous Enhancement and Quenching of the Excited States of Silver Nanoclusters. *J Phys Chem C.* **2019**, *123*, 14921-14927.

[31] Bootharaju, M. S.; Kozlov, S. M.; Cao, Z.; Harb, M.; Maity, N.; Shkurenko, A.; Parida, M. R.; Hedhili, M. N.; Eddaoudi, M.; Mohammed, O. F.; Bakr, O. M.; Cavallo, L.; Basset, Doping-Induced Anisotropic Self-Assembly of Silver Icosahedra in $[Pt_2Ag_{23}Cl_7(PPh_3)_{10}]$ Nanoclusters. J. M. *J Am Chem Soc.* **2017**, *139*, 1053-1056.

[32] Gromov, D. G.; Pyatilova, O. V.; Bulyarskii, S. V.; Belov, A. N.; Raskin, A. A. Specific features of the formation of arrays of silver clusters from a thin film on a SiO_2 surface. *Phys Solid State.* **2013**, *55*, 619-623.

[33] Huang, R. W.; Wei, Y. S.; Dong, X. Y.; Wu, X. H.; Du, C. X.; Zang, S. Q.; Mak, T. C. W. Hypersensitive dual-function luminescence switching of a silver-chalcogenolate cluster-based metal-organic framework. *Nat Chem.* **2017**, *9*, 689-697.

[34] Sheldrick, G. M. SADABS: Program for Area Detector Adsorption Correction; University of Göttingen: Göttingen, Germany, **1996**.

[35] Sheldrick, G. M. *SHELXL-2014/7*: A Program for Structure Refinement; University of Göttingen: Göttingen, Germany, **2014**.

[36] Dolomanov, O. V.; Bourhis, L. J.; Gildea, R. J.; J. Howard, A. K.; Puschmann, H. *OLEX2*: a complete structure solution, refinement and analysis program. *J. Appl. Cryst.* **2009**, *42*, 339-341.

[37] Van der Sluis, P.; Spek, A. L. Acta Crystallogr., Sect. A: Found. *Crystallogr.* **1990**, *46*, 194–201.

[38] Wang, Q. M.; Lin, Y. M.; Liu, K. G. Role of Anions Associated with the Formation and Properties of Silver Clusters. *Acc Chem Res.* **2015**, *48*, 1570-1579.

[39] Wang, Z.; Li, X. Y.; Liu, L. W.; Yu, S. Q.; Feng, Z. Y.; Tung, C. H.; Sun, D. *Chem. Eur. J.* **2016**, *22*, 6830-6836.

[40] Jin, J. L.; Shen, Y. L.; Xie, Y. P.; Lu, X. Anion Templated Synthesis of Silver(I)-Ethynide Dithiophosphate Clusters. *Cryst Growth Des.* **2018**, *18*, 4372-4377.

[41] Bian, S. D.; Wu, H. B.; Wang, Q. M. A Facile Template Approach to High - Nuclearity Silver(I) Alkynyl Clusters. *Angew. Chem. Int. Ed.* **2009**, *48*, 5363-5365.

[42] Li, Y. L.; Xu, Q. Q.; Li, S.; Huang, R. W.; Liu, X. F.; Wei, Y. L.; Zang, S. Q. Investigating the influence of a $CrO_4^{2-}/Cr_2O_7^{2-}$ template in the formation of a series of silver–chalcogenide clusters. *New J Chem.* **2019**, *43*, 115-120.

[43] Wang, Z.; Zhuo, H. Y.; Hu, A. Y.; Su, H. F.; Zhao, Q. Q.; Wang, X. P.; Tung, C. H.; Sun, D. Self-Assembly of A Novel Ag_{48} Cluster Encapsulating an Unprecedented $[Mo_8O_{28}]^{8-}$ Anion Template. *Isr. J. Chem.* **2018**, *59*, 280-285.

[44] Wang, Z.; Liu, J. W.; Su, H. F.; Zhao, Q. Q.; Kurmoo, M.; Wang, X. P.; Tung, C. H.; Sun, D.; Zheng, L. S. Chalcogens-Induced $Ag_6Z_4@Ag_{36}$ (Z = S or Se) Core–Shell Nanoclusters: Enlarged Tetrahedral Core and Homochiral Crystallization. *J Am Chem Soc.* **2019**, *141*, 17884-17890.

[45] Desireddy, A.; Conn, B. E.; Guo, J.; Yoon, B.; Barnett, R. N.; Monahan, B. M.; Kirschbaum, K.; Griffith, W. P.; Whetten, R. L.; Landman, U.; Bigioni, T. P. Ultrastable silver nanoparticles. *Nature* **2013**, *501*, 399-402.

[46] Fang, W. H.; Zhang, L.; Zhang, J. A 3.6 nm Ti_{52}–Oxo Nanocluster with Precise Atomic Structure. *J Am Chem Soc.* **2016**, *138*, 7480-7483.

[47] Gao, M. Y.; Zhang, L.; Zhang, J. Acid-Controlled Synthesis of Carboxylate-Stabilized Ti_{44}-Oxo Clusters: Scaling up Preparation, Exchangeable Protecting Ligands, and Photophysical Properties. *Chem. Eur. J.* **2019**, *25*, 1-7.

[48] Malay, A. D.; Miyazaki, N.; Biela, A.; Chakraborti, S.; Majsterkiewicz, K.; Stupka, I.; Kaplan, C. S.; Kowalczyk, A.; Piette, B. M. A. G.; Hochberg, G. K. A.; Wu, D.; Wrobel, T. P.; Fineberg, A.; Kushwah, M. S.; Kelemen, M.; Vavpetič, P.; Pelicon, P.; Kukura, P.; Benesch, J. L. P.; Iwasaki, K.; Heddle, J. G. An ultra-stable gold-coordinated protein cage displaying reversible assembly. *Nature* **2019**, *569*, 438-442.

[49] Li, S.; Wang, Z. Y.; Gao, G. G.; Li, B.; Luo, P.; Kong, Y. J.; Liu, H.; Zang, S. Q. Smart Transformation of a Polyhedral Oligomeric Silsesquioxane Shell Controlled by Thiolate Silver(I) Nanocluster Core in Cluster@Clusters Dendrimers. *Angew. Chem. Int. Ed.* **2018**, *57*, 12775-12779.

[50] Wang, Z.; Su, H. F.; Kurmoo, M.; Tung, C. H.; Sun, D.; Zheng, L. S. Trapping an octahedral Ag_6 kernel in a seven-fold symmetric Ag_{56} nanowheel. *Nat Commun.* **2018**, *9*, 2094.

[51] Yang, H.; Yan, J.; Wang, Y.; Su, H.; Gell, L.; Zhao, X.; Xu, C.; Teo, B. K.; Häkkinen, H.; Zheng, N. Embryonic Growth of Face-Center-Cubic Silver Nanoclusters Shaped in Nearly Perfect Half-Cubes and Cubes. *J Am Chem Soc.* **2017**, *139*, 31-34.

[52] Xie, Y. P.; Jin, J. L.; Lu, X.; Mak, T. C. W. High-Nuclearity Silver Thiolate Clusters Constructed with Phosphonates. *Angew. Chem. Int. Ed.* **2015**, *54*, 15176-15180.

[53] Liu, J. W.; Feng, L.; Su, H. F.; Wang, Z.; Zhao, Q. Q.; Wang, X. P.; Tung, C. H.; Sun, D.; Zheng, L. S. Anisotropic Assembly of Ag_{52} and Ag_{76} Nanoclusters. *J Am Chem Soc.* **2018**, *140*, 1600-1603.

[54] Anson, C. E.; Eichhöfer, A.; Issac, I.; Fenske, D.; Fuhr, O.; Sevillano, P.; Persau, C.; Stalke, D.; Zhang, J. Synthesis and Crystal Structures of the Ligand-Stabilized Silver Chalcogenide Clusters $[Ag_{154}Se_{77}(dppxy)_{18}]$, $[Ag_{320}(StBu)_{60}S_{130}(dppp)_{12}]$, $[Ag_{352}S_{128}(StC_5H_{11})_{96}]$, and $[Ag_{490}S_{188}(StC_5H_{11})_{114}]$. *Angew. Chem. Int. Ed.* **2008**, *47*, 1326-1331.

SYNOPSIS TOC